Article:
de Borst, R. orcid.org/0000-0002-3457-3574 and Verhoosel, C.V. (2016) Gradient damage vs phase-field approaches for fracture: Similarities and differences. Computer Methods in Applied Mechanics and Engineering, 312. pp. 78-94. ISSN 0045-7825

https://doi.org/10.1016/j.cma.2016.05.015

Gradient damage *vs* phase-field approaches for fracture: similarities and differences

René de Borst[1,*], Clemens V. Verhoosel[b]

[a] *University of Sheffield, Department of Civil and Structural Engineering, Mappin Street, Sir Frederick Mappin Building, Sheffield A1 3JD, UK*
[b] *Eindhoven University of Technology, Department of Mechanical Engineering, P.O. Box 513, 5600MB Eindhoven, Netherlands*

Abstract

Gradient-enhanced damage models and phase-field models are seemingly very disparate approaches to fracture. Whereas gradient-enhanced damage models find their roots in damage mechanics, which is a smeared approach from the onset, and gradients were added to restore well-posedness beyond a critical strain level, the phase-field approach to brittle fracture departs from a discontinuous description of failure, where the distribution function is regularised, leading to the inclusion of spatial gradients as well. Herein, we will consider both approaches, and discuss their similarities and differences. The averaging (diffusion) equations for the averaging field and the phase-field will be compared, and it is shown that the diffusion equation for the phase-field can be conceived as a special case of the averaging equation of a gradient-damage model where the damage is averaged. Further, the role of the driving force is examined, and it is shown that subtle differences in the degradation functions commonly adopted in damage and phase-field approaches are key to the observation that, different from damage mechanics, the fracture process zone does not broaden in the wake of the crack tip.

Keywords: fracture, damage, gradient models, phase-field approach

1. Introduction

The numerical modelling to fracture can be approached from two different points of view. Discrete models for fracture, where the geometrical discontinuity is modelled as such, i.e. by modifying the geometry of the original, intact structure, are perhaps intuitively the most appealing approach to fracture, and have been pursued since the late 1960s [1]. Developments such as remeshing [2, 3], or the eXtended Finite Element Method [4, 5, 6, 7, 8] have provided ways to decouple the crack path from the underlying discretisation. Also, isogeometric finite element analysis behold promise to flexibly model propagating cracks [9].

[*] Corresponding author: René de Borst
Email address: r.deborst@sheffield.ac.uk (René de Borst)

Nevertheless, issues remain such as the proper modelling of curved crack fronts in three dimensions, while the robust implementation of discrete cracks in a three-dimensional setting is a non-trivial task, either when using remeshing, or when exploiting the partition of unity concept as in the eXtended Finite Element Method. Hence, smeared, or distributed, crack approaches have been put forward, where the discontinuity is distributed over a finite width. Another interpretation is that the Dirac function that arises for the strain at a discontinuity is replaced by a smooth function. The smearing out of the discontinuity is accompanied by the introduction, at local continuum level, of a stress-strain relation in which the limit strength is gradually reduced. The strain-softening that is introduced in this manner, however, locally leads to a change of the character of the governing partial differential equations: loss of ellipticity in case of quasi-static analyses, and loss of hyperbolicity for dynamic calculations.

This change causes a loss of well-posedness of the rate boundary value problem, which in turn causes a complete dependence of the numerical results on the discretisation, not only with respect to mesh refinement but also, and especially, with respect to mesh alignment, since failure zones exhibit a strong tendency to propagate along lines of discretisation. This tendency can be ameliorated by using elements in which the kinematics have been enriched by locally adding shape functions that can capture a discontinuity, e.g. [10, 11, 12, 13]. However, to avoid loss of well-posedness, the standard, rate-independent continuum must be enhanced. Several possibilities exist: adding viscosity, e.g. [14, 15], adding couple stresses and conjugate kinematic quantities like microcurvatures, micromorphic continua with the Cosserat continuum as the classical example [16], see [17, 18] for a numerical implementation of Cosserat elasto-plasticity, spatial averaging [19], and the introduction of a dependence on spatial strain gradients, e.g. [20, 21] for gradient plasticity, and [22, 23, 24, 25] for gradient-enhanced damage models. Especially the latter class of models has become popular for computational analysis.

Another class of continuum descriptions of cracking has been developed in the context of brittle fracture. Pioneering work has been done by [26, 27, 28], who proposed a phase-field approximation of the variational formulation for Griffith's theory of brittle fracture based on the Mumfort-Shah potential [29]. A more mechanically oriented formulation, which, however closely resembles the mentioned developments, has been derived by [30, 31]. Subsequently, phase-field models have been applied to a large variety of fracture problems, including dynamic problems [32, 33] and cohesive fracture [34].

However, the point of departure of both models is different. In gradient damage models intrinsically a mechanical approach is adopted, and the damage model is regularised by adding gradients to restore well-posedness of the boundary value problem in the post-peak regime. The basic idea of phase-field models, on the other hand, is to replace the zero-width discontinuity by a small, but finite zone with sharp gradients in a mathematically consistent manner. Indeed, the latter requirement inevitably leads to the inclusion of spatial derivatives in the energy functional, similar to gradient damage models.

To provide a proper setting we start by giving a brief outline of damage models, and their extension to nonlocality. An important issue in gradient damage models is the observation that in the wake of the crack tip there is a broadening of the damage

field. To eliminate this broadening it has been proposed to make the internal length scale parameter a function of the local strain or damage level [35]. Next, a brief review of the phase-field approach to brittle fracture is given, and the different point of departure is emphasised. It is recalled that in this approach no broadening is observed of the damage zone. It is also argued that the regularisation parameter and the degradation function that are introduced are, in fact, material parameters, and have to be calibrated to experiments. A discussion on the differences and similarities between gradient-enhanced damage models and the phase-field approach to brittle fracture follows, including a comparison of the various formats of the diffusion equation for the damage/phase field that ensues for the different formulations and a discussion of the importance of the specific form of the driving force for the broadening of the damage zone.

2. Nonlocal and gradient-enhanced damage models

2.1. Damage models

Herein, we restrict ourselves to an isotropic damage evolution, which is characterised by a total stress-strain relation:

$$\boldsymbol{\sigma} = (1-d_1)E\left(\frac{(1-d_2)\nu}{(1+(1-d_2)\nu)(1-2(1-d_2)\nu)}\boldsymbol{i}\otimes\boldsymbol{i} + \frac{1}{1+(1-d_2)\nu}\mathbf{I}\right) : \boldsymbol{\epsilon} \quad (1)$$

with $\boldsymbol{i}$ the second-order identity tensor, $\mathbf{I}$ the fourth-order identity tensor, E the Young's modulus and ν the Poisson ratio, which are degraded by the scalar damage variables d_1 and d_2, respectively. A simplification is obtained by assuming the Poisson ratio to remain constant during the damage process, so that:

$$\boldsymbol{\sigma} = (1-d)\mathbf{D}^e : \boldsymbol{\epsilon} \quad (2)$$

with d a scalar damage variable which grows from zero to one (at complete loss of integrity) and $\mathbf{D}^e$ the fourth-order elastic stiffness tensor. For strain-based damage models, the total stress-strain relation, Equation (2), is complemented by a damage loading function

$$f = f(\tilde{\epsilon}, \kappa) \quad (3)$$

with $\tilde{\epsilon}$ a scalar-valued function of the strain tensor, and κ a history variable. The damage loading function f and the rate of the history variable, $\dot{\kappa}$, have to satisfy the discrete Kuhn-Tucker loading-unloading conditions

$$f \leq 0\ ,\ \dot{\kappa} \geq 0\ ,\ \dot{\kappa} f = 0 \quad (4)$$

The history parameter κ starts at a damage threshold level κ_i and is updated by the requirement that during damage growth $f = 0$. Damage growth occurs according to an evolution equation, such that:

$$d = d(\kappa) \quad (5)$$

which can be inferred from a uniaxial test.

2.2. Nonlocal damage models

In a nonlocal generalisation, the equivalent strain $\tilde{\epsilon}$ is normally replaced by a spatially averaged quantity in the damage-loading function [19]:

$$f(\bar{\epsilon}, \kappa) = \bar{\epsilon} - \kappa \tag{6}$$

where the nonlocal strain $\bar{\epsilon}$ is computed from

$$\bar{\epsilon}(\mathbf{x}) = \frac{1}{\Psi(\mathbf{x})} \int_\Omega \psi(\mathbf{y}, \mathbf{x}) \tilde{\epsilon}(\mathbf{y}) \, \mathrm{d}\Omega, \quad \Psi(\mathbf{x}) = \int_\Omega \psi(\mathbf{y}, \mathbf{x}) \, \mathrm{d}\Omega \tag{7}$$

with $\psi(\mathbf{y}, \mathbf{x})$ a weight function. Often, the weight function is assumed to be homogeneous and isotropic, so that it only depends on the norm

$$r = \|\mathbf{x} - \mathbf{y}\| \tag{8}$$

In this formulation, all the other relations remain local: the local stress-strain relation, Equation (2), the loading-unloading conditions, Equation (4), and the dependence of the damage variable d on the history parameter, Equation (5). As an alternative to Equation (7), the local history parameter κ may be replaced in the damage-loading function f by a spatially averaged quantity $\bar{\kappa}$, such that

$$f(\epsilon, \bar{\kappa}) = \epsilon - \bar{\kappa} \tag{9}$$

where

$$\bar{\kappa}(\mathbf{x}) = \frac{1}{\Psi(\mathbf{x})} \int_\Omega \psi(\mathbf{y}, \mathbf{x}) \kappa(\mathbf{y}) \, \mathrm{d}\Omega \tag{10}$$

2.3. Gradient-enhanced damage models

Nonlocal constitutive relations can be considered as a point of departure for constructing gradient models, although we wish to emphasise that the latter class of models can also be defined directly by supplying higher-order gradients in the damage-loading function. Yet, we will follow the first-mentioned route to underline the connection between integral and differential-type nonlocal models. This is done either by expanding the kernel $\tilde{\epsilon}$ of the integral in Equation (7) in a Taylor series, or by expanding of the history parameter κ in Equation (10) as a Taylor series. If we truncate after the second-order terms and carry out the integration implied in Equation (7) under the assumption of isotropy, the following relation ensues:

$$\bar{\epsilon} = \tilde{\epsilon} + g \nabla^2 \tilde{\epsilon} \tag{11}$$

where g is a gradient parameter of the dimension length squared.

Equation (11) bears the disadvantage that it requires the computation of second-order gradients of the local equivalent strain $\tilde{\epsilon}$. Since this quantity is a function of the strain tensor, and since the strain tensor involves first-order derivatives of the displacements, third-order derivatives of the displacements have to be computed, which

would necessitate C^2-continuity of the shape functions. To obviate this problem, Equation (11) is differentiated twice and the result is substituted again into Equation (11). Again neglecting fourth-order terms leads to

$$\bar{\epsilon} - g\nabla^2\bar{\epsilon} = \tilde{\epsilon} \tag{12}$$

In [25], see also [30], it has been shown that the implicit gradient formulation, Equation (12), becomes formally identical to a fully nonlocal formulation when, in three dimensions, the weighting function is chosen as

$$\psi(\mathbf{y}, \mathbf{x}) = \frac{1}{4\pi g r} \exp\left(-\frac{r}{\sqrt{g}}\right) \tag{13}$$

Indeed, the 'implicit gradient' formulation has a truly nonlocal character, which is different from the 'explicit gradient' formulation, Equation (11).

In a fashion similar to the derivation of the gradient-damage models based on the averaging of the equivalent strain $\tilde{\epsilon}$, we can elaborate a gradient approximation of Equation (10), i.e. by developing $\bar{\kappa}$ in a Taylor series. For an isotropic, infinite medium, and truncating after the second term, we have [23]:

$$\bar{\kappa} = \kappa + g\nabla^2\kappa \tag{14}$$

Similar to the second-order gradient model where the nonlocal strain has been expanded, an 'implicit' version can be developed by differentiating Equation (14) twice and substituting the result back into Equation (14). Neglecting fourth-order terms then yields:

$$\bar{\kappa} - g\nabla^2\bar{\kappa} = \kappa \tag{15}$$

A spatially averaged damage field $\bar{d}$ is now defined as a function of $\bar{\kappa}$: $\bar{d} = \bar{d}(\bar{\kappa})$. Taking the special case of a linear relation between $\bar{d}$ and $\bar{\kappa}$ [23, 24]:

$$\bar{d} = \bar{\kappa}_0 + a\bar{\kappa} \tag{16}$$

Equation (15) becomes

$$\bar{d} - \frac{g}{a}\nabla^2\bar{d} = \bar{\kappa}_0 + a\kappa \tag{17}$$

or, setting $d = \bar{\kappa}_0 + a\kappa$ and $g' = g/a$,

$$\bar{d} - g'\nabla^2\bar{d} = d \tag{18}$$

In the remainder the prime will be omitted for notational convenience – noting that the gradient parameter g will have a different meaning depending on the exact gradient formulation – and we will write for the averaging equation of the nonlocal damage field:

$$\bar{d} - g\nabla^2\bar{d} = d \tag{19}$$

2.4. Discrete format of gradient-damage models

Numerical schemes for gradient-enhanced continua typically have the character of a coupled problem and commonly depart from the weak form of the balance of momentum,

$$\int_\Omega \nabla^{\text{sym}}\boldsymbol{\eta} : \boldsymbol{\sigma}\, \mathrm{d}\Omega = \int_\Gamma \boldsymbol{\eta} \cdot \bar{\mathbf{t}}\, \mathrm{d}\Gamma \tag{20}$$

with $\boldsymbol{\eta}$ the test function for the displacements and $\bar{\mathbf{t}}$ the prescribed boundary tractions, and a weak form of the averaging equation. For example, for the strain-based implicit gradient damage model, Equation (12), one has:

$$\int_\Omega \zeta(\bar{\epsilon} - g\nabla^2\bar{\epsilon} - \tilde{\epsilon})\, \mathrm{d}\Omega = 0 \tag{21}$$

with ζ the test function for the nonlocal strain $\bar{\epsilon}$. Transforming Equation (21) using the divergence theorem and the natural boundary condition $\mathbf{n}_\Gamma \cdot \nabla\bar{\epsilon} = 0$, with $\mathbf{n}_\Gamma$ the normal to the external boundary Γ, yields:

$$\int_\Omega (\zeta\bar{\epsilon} + g\nabla\zeta \cdot \nabla\bar{\epsilon})\, \mathrm{d}\Omega = \int_\Omega \zeta\tilde{\epsilon}\ \mathrm{d}\Omega \tag{22}$$

The displacements $\mathbf{u}$ and the nonlocal strains $\bar{\epsilon}$ are discretised as:

$$\mathbf{u} = \mathbf{N}\mathbf{a} \quad \text{and} \quad \bar{\epsilon} = \bar{\mathbf{N}}\mathbf{e} \tag{23}$$

with $\mathbf{N}$ and $\bar{\mathbf{N}}$ containing the interpolation polynomials. In a Bubnov-Galerkin approach we have for the test functions

$$\boldsymbol{\eta} = \mathbf{N}\mathbf{w} \quad \text{and} \quad \zeta = \bar{\mathbf{N}}\mathbf{z} \tag{24}$$

Substitution into Equations (20) and (22), and requiring that the result holds for arbitrary $(\mathbf{w}, \mathbf{z})$ yields the discrete formats of the equilibrium equation:

$$\int_\Omega \mathbf{B}^{\mathrm{T}}\boldsymbol{\sigma}\, \mathrm{d}\Omega = \int_\Gamma \mathbf{N}^{\mathrm{T}}\mathbf{t}_p\ \mathrm{d}\Gamma \tag{25}$$

and the averaging equation:

$$\int_\Omega (\bar{\mathbf{N}}^{\mathrm{T}}\bar{\mathbf{N}} + g(\nabla\bar{\mathbf{N}})^{\mathrm{T}}\nabla\bar{\mathbf{N}})\, \mathrm{d}\Omega = \int_\Omega \bar{\mathbf{N}}^{\mathrm{T}}\tilde{\boldsymbol{\epsilon}}\ \mathrm{d}\Omega \tag{26}$$

The tangent stiffness matrix needed for an iterative solution via the Newton-Raphson method reads [22]:

$$\begin{bmatrix} \mathbf{K}_{aa} & \mathbf{K}_{ae} \\ \mathbf{K}_{ea} & \mathbf{K}_{ee} \end{bmatrix} \begin{pmatrix} \mathrm{d}\mathbf{a} \\ \mathrm{d}\mathbf{e} \end{pmatrix} = \begin{pmatrix} \mathbf{f}_a^{\text{ext}} - \mathbf{f}_a^{\text{int}} \\ \mathbf{f}_e^{\text{int}} - \mathbf{K}_{ee}\mathbf{e} \end{pmatrix} \tag{27}$$

with $\mathbf{f}_e^{\text{int}}$ given by the right-hand side of Equation (26). The stiffness matrices are given by

$$\mathbf{K}_{aa} = \int_\Omega (1-d)\mathbf{B}^{\mathrm{T}}\mathbf{D}^{\mathrm{e}}\mathbf{B}\,\mathrm{d}\Omega \tag{28}$$

$$\mathbf{K}_{ae} = \int_\Omega q\mathbf{B}^{\mathrm{T}}\mathbf{D}^{\mathrm{e}}\boldsymbol{\epsilon}\bar{\mathbf{N}}\,\mathrm{d}\Omega \tag{29}$$

$$\mathbf{K}_{ea} = \int_\Omega \bar{\mathbf{N}}^{\mathrm{T}}\left(\frac{\partial\tilde{\epsilon}}{\partial\boldsymbol{\epsilon}}\right)\mathbf{B}\,\mathrm{d}\Omega \tag{30}$$

$$\mathbf{K}_{ee} = \int_\Omega \left(\bar{\mathbf{N}}^{\mathrm{T}}\bar{\mathbf{N}} + g(\nabla\bar{\mathbf{N}})^{\mathrm{T}}\nabla\bar{\mathbf{N}}\right)\,\mathrm{d}\Omega \tag{31}$$

where $q = \frac{\partial d}{\partial \kappa}$ for loading and vanishes otherwise.

In the above we have restricted the discussion to the case of the second-order implicit gradient-damage model. Unlike for this second-order approximation to the nonlocal damage model, an order reduction such that C^0-continuous shape functions suffice for the interpolation of the additional independent variables can generally not be achieved for higher-order approximations. For instance, when the fourth-order term is retained, so that the averaging equation (12) is replaced by

$$\bar{\epsilon} - g_1\nabla^2\bar{\epsilon} - g_2\nabla^4\bar{\epsilon} = \tilde{\epsilon} \tag{32}$$

with g_1 and g_2 two gradient constants, C^1-continuous shape functions are necessary for the interpolation of the nonlocal strain $\bar{\epsilon}$. When incorporating the sixth-order term C^2-continuity is required, etc.

2.5. Broadening of the damage zone

We now consider the three-point bending beam of Figure 1 [36]. The beam has the dimensions $2000 \times 300\,\mathrm{mm}^2$ and a thickness of 50 mm. It is supported by hinges on the left and right bottom corners, and is loaded by a distributed load $\bar{t}$ over the central section (100 mm) of the specimen.

A linear isotropic material is considered with modulus of elasticity $E = 20\,\mathrm{GPa}$ in the undamaged state and Poisson's ratio $\nu = 0.2$. Plane-strain conditions have been assumed, and the local equivalent strain is given by:

$$\eta(\epsilon) = \sqrt{\langle\epsilon_i\rangle^2} = \sqrt{\langle\epsilon_1\rangle^2 + \langle\epsilon_2\rangle^2} \tag{33}$$

where ϵ_1 and ϵ_2 are the principal strains, and the Macaulay brackets distinguish between tension and compression. The damage law proposed in Reference [35] has been used:

$$d(\kappa) = \begin{cases} 0 & \kappa \le \kappa_0 \\ 1 - \frac{\kappa_0}{\kappa}\left\{(1-\alpha) + \alpha\exp\left[\beta(\kappa_0 - \kappa)\right]\right\} & \kappa > \kappa_0 \end{cases} \tag{34}$$

with $\kappa_0 = 10^{-4}$, $\alpha = 0.99$ and $\beta = 500$. The gradient parameter is taken as $g = 200\,\mathrm{mm}^2$.

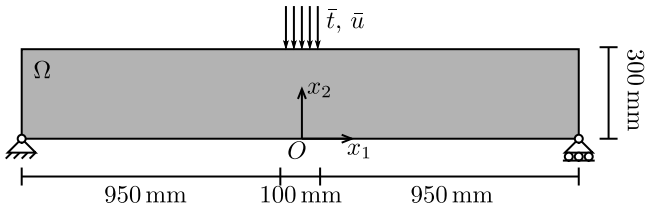

Figure 1: Three-point bending specimen. The thickness of the specimen is 50 mm

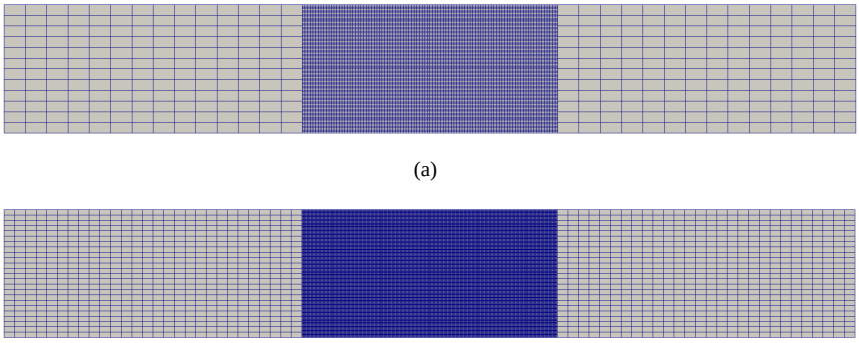

(a)

(b)

Figure 2: Meshes for the three-point bending specimen: Coarse mesh with 2,388 elements and fine mesh with 9,552 elements

The computations have been done on the quadrilateral meshes of Figure 2. In the central region of the beam, where the damage zone will evolve, hierarchical refinements [37] have been used to improve the resolution. Because the mesh is refined hierarchically, the elements in the central region can be kept square. The total number of degrees of freedom with bilinear basis functions for both the displacement field and damage field is 7,246 for the coarse mesh and 28,816 for the fine mesh.

A force F is defined as the distributed load $\bar{t}$ times the area to which it has been applied. The displacement $\bar{u}$ has been taken as the average downward displacement of the loading region, see Figure 1. This displacement has been used as the constraint in the path-following method used to trace the equilibrium path. The results obtained for the second-order gradient formulation are shown in Figure 3. As can be seen, the results obtained using the coarse mesh are in good agreement with that of the fine mesh.

It is observed from Figure 4 that, upon propagation of the damage zone, it not only extends, but also broadens. In Figure 5 the damage is plotted over the line $x_1 \in [-300\,\text{mm}, 300\,\text{mm}]$ and $x_2 = 50\,\text{mm}$ at various stages of the loading process (measured by the downward deflection $\bar{u}$). The broadening effect is clearly visible from the $d = 0.95$ contour line, and is observed to be insensitive to the mesh size. This artefact was first observed in [35] and makes standard gradient damage formulations less suitable to mimick a sharp crack. As indicated in [35] the broadening effect is a consequence of the continued increase of the local and nonlocal equivalent strain af-

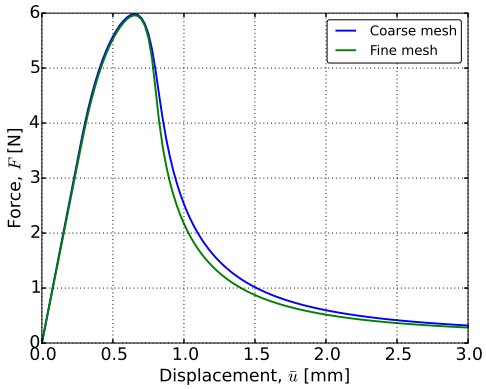

Figure 3: Mesh convergence study for the three-point bending beam using the second-order gradient formulation, discretised using the meshes shown in Figure 2

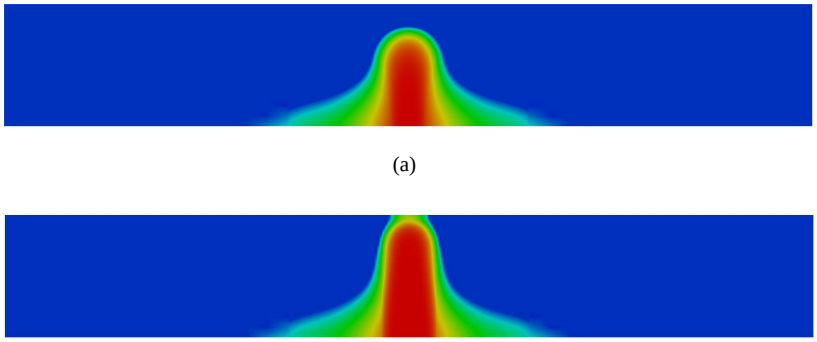

(a)

(b)

Figure 4: Damage profiles for (a) $\bar{u} = 0.875\,\text{mm}$, and (b) $\bar{u} = 2.00\,\text{mm}$ obtained using the second-order gradient formulation. Undamaged material is indicated in blue, fully damaged material in red

ter damage has fully developed. For the three-point bending test considered here, this phenomenon is visualised in Figure 6.

In Figure 7 the broadening phenomenon is shown again, but now for the case that the internal length scale of the damage formulation has been decreased by a factor 2 (so that the gradient parameter g has been decreased by a factor 4), and where use has been made of the fine mesh of Figure 2. Figure 8 shows the broadening effect for the damage field and the corresponding behavior of the local and the smoothed equivalent strain fields. The results show that for a smaller internal length scale the width of the damage zone has decreased, but that the broadening effect remains. Indeed, the problem can only be remedied by making the internal length scale a function of the local equivalent strain. This, however, increases the computational effort [35].

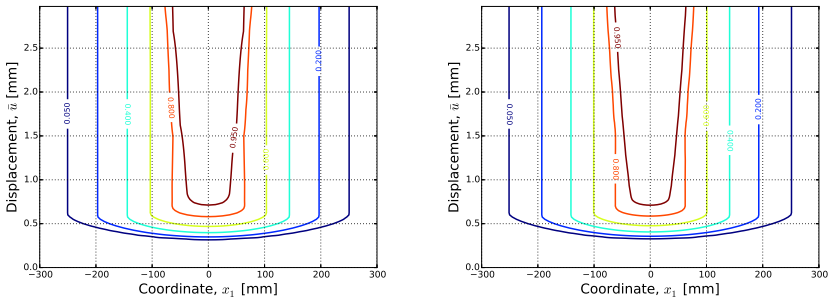

Figure 5: Evolution of the damage profile along the line $x_1 \in [-300\,\text{mm}, 300\,\text{mm}]$ and $x_2 = 50\,\text{mm}$ as the downward deflection of the loading boundary, $\bar{u}$, increases, for the coarse (left) and the fine (right) meshes

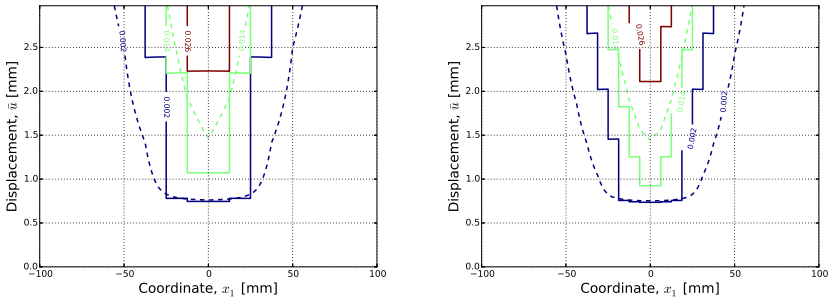

Figure 6: Evolution of the local (solid) and smoothed (dashed) equivalent strain profiles for both meshes along the line $x_1 \in [-100\,\text{mm}, 100\,\text{mm}]$ and $x_2 = 50\,\text{mm}$ as the downward deflection of the loading boundary, $\bar{u}$, increases, for the coarse (left) and the fine (right) meshes

3. The phase-field approach to brittle fracture

3.1. Formulation

The basic idea of phase-field models is to approximate a discontinuity Γ by a smeared surface Γ_ℓ. In a one-dimensional setting the exponential function

$$\bar{d}(x) = e^{-\frac{|x|}{2\ell}} \tag{35}$$

is used to approximate the discontinuous function of Figure 9(a), with ℓ the internal length scale parameter. The phase-field variable $\bar{d} \in [0, 1]$ describes the phase field. Following the earlier discussion on gradient-enhanced damage models, the bar indicates that a regularised (or spatially averaged) quantity is considered, and $\bar{d}$ is defined such that $\bar{d} = 0$ characterises the intact state of the material, while $\bar{d} = 1$ represents the fully broken material, similar to the definition commonly adopted in damage mechanics. In one dimension, Equation (35) is the solution to:

$$\bar{d} - 4\ell^2 \bar{d}_{,xx} = 0 \tag{36}$$

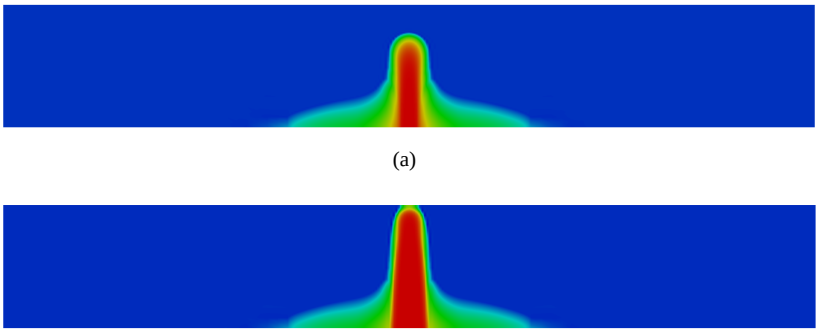

(a)

(b)

Figure 7: Damage profiles for (a) $\bar{u} = 0.625\,\text{mm}$, and (b) $\bar{u} = 2.00\,\text{mm}$ obtained using the second-order gradient formulation, but with the internal length scale decreased by a factor 2, so that the gradient parameter has decreased by a factor 4 ($g = 50\ \text{mm}^2$)

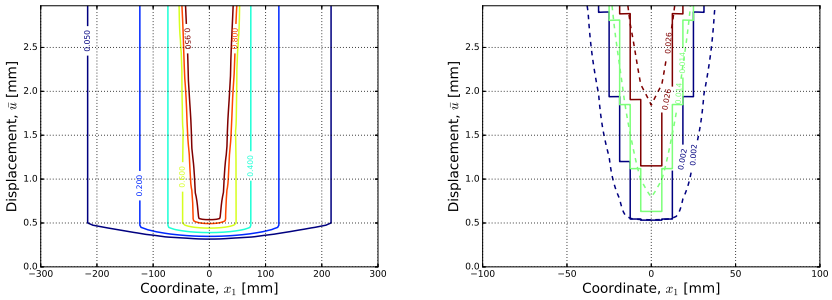

Figure 8: Evolution of the damage profile (left), and the local (solid) and smoothed (dashed) equivalent strain profiles (right) along the line $x_1 \in [-300\,\text{mm}, 300\,\text{mm}]$ and $x_2 = 50\,\text{mm}$ as the downward deflection, $\bar{u}$, of the loading boundary (fine mesh and $g = 50\ \text{mm}^2$)

where a comma denotes differentiation, subject to the boundary conditions: $\bar{d}(0) = 1$ and $\bar{d}(\pm\infty) = 0$. This can be demonstrated simply by applying the Ansatz function $\bar{d} = e^{-|\lambda||x|}$ to Equation (36), solving for λ and subsequently using the boundary conditions to determine the constant parameter. Using Equation (36) the discontinuity Γ can be approximated by the functional Γ_ℓ

$$\Gamma_\ell = \int_\Omega \underbrace{\frac{1}{4\ell}\left(\bar{d}^2 + 4\ell^2 \bar{d}_{,x}^2\right)}_{\gamma_\ell} \,\mathrm{dV} \tag{37}$$

with γ_ℓ the crack surface density function, see [30] for details. In a multi-dimensional setting γ_ℓ can be expanded as follows:

$$\gamma_\ell = \frac{1}{4\ell}\left(\bar{d}^2 + 4\ell^2 \nabla\bar{d}\cdot\nabla\bar{d}\right) \tag{38}$$

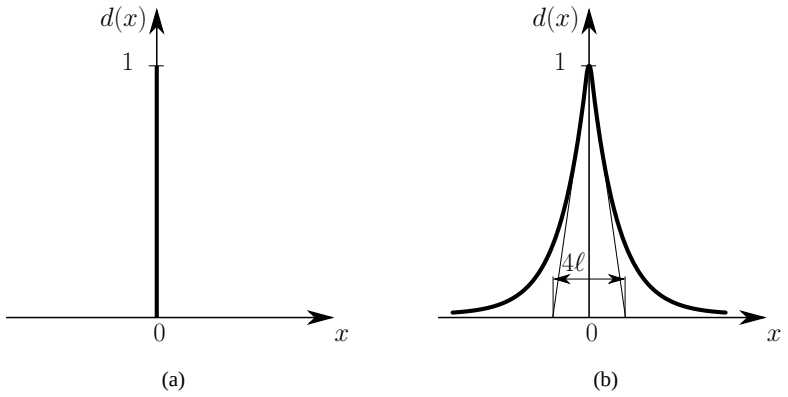

Figure 9: (a) A sharp crack, and (b) smeared crack modelled with the length scale parameter ℓ

We consider a volume Ω with an internal discontinuity boundary Γ_d. As a starting point we consider the potential energy for the case of a discrete description of brittle fracture in the Griffith sense [26]:

$$\Psi_{\text{pot}} = \int_{\Omega} \psi^e(\boldsymbol{\epsilon})\,\mathrm{d}V + \int_{\Gamma_d} \mathcal{G}_c\,\mathrm{d}A \tag{39}$$

with the elastic energy density ψ^e a function of the infinitesimal strain tensor $\boldsymbol{\epsilon}$: $\psi^e = \psi^e(\boldsymbol{\epsilon})$. The elastic energy density is expressed by Hooke's law for an isotropic linear elastic material as $\psi^e(\boldsymbol{\epsilon}) = \frac{1}{2}\lambda\epsilon_{ii}\epsilon_{jj} + \mu\epsilon_{ij}\epsilon_{ij}$, with λ and μ the Lamé constants, and the summation convention applies. In Equation (39) the fracture energy, i.e. the amount of energy dissipated upon the creation of a unit of fracture surface, is denoted by $\mathcal{G}_c$. In the spirit of a regularised crack topology, the work required to create a unit crack area is expressed as a volume integral which depends on the phase field variable $\bar{d}$ and the fracture energy $\mathcal{G}_c$:

$$\int_{\Gamma_d} \mathcal{G}_c \mathrm{d}A \approx \int_{\Omega} \mathcal{G}_c \gamma_\ell(\bar{d}, \nabla\bar{d})\,\mathrm{d}V. \tag{40}$$

The next step is inspired by damage mechanics concepts and relies on the assumption that the evolution of the phase field is directly related to crack growth. As such, it can be thought of as a way to model the loss of stiffness of the bulk of the solid. For this purpose a degradation function $h = h(\bar{d})$ is introduced, which must satisfy the following conditions:

$$\begin{cases} h : [0,1] \to [0,1] \\ h(0) = 1 \quad , \quad h(1) = 0 \\ h'(\bar{d}) < 0 \quad \bar{d} \in [0,1[\\ h'(1) = 0 \end{cases} \tag{41}$$

These properties ensure damage propagation and provide an upper bound to the phase field $\bar{d}$ variable of one [31]. A quadratic polynomial is widely used:

$$h(\bar{d}) = (1 - \bar{d})^2 \tag{42}$$

In [27] the degradation function h was multiplied with the elastic energy density of the undamaged state, ψ_0, such that the elastic energy density of the damaged state reads:

$$\psi^e(\boldsymbol{\epsilon}, \bar{d}) = h(\bar{d})\psi_0(\boldsymbol{\epsilon}) \tag{43}$$

This formulation was refined to account for the fact that damage evolution occurs under different straining modes [30, 38], and it was assumed that the elastic energy of the undamaged state can be additively decomposed into a damaged and an intact part, $\psi_0 = \psi_0^d + \psi_0^i$, such that the degradation function h only acts on the damaged part:

$$\psi^e(\boldsymbol{\epsilon}, \bar{d}) = h(\bar{d})\psi_0^d(\boldsymbol{\epsilon}) + \psi_0^i(\boldsymbol{\epsilon}) \tag{44}$$

Substitution of Equations (40) and (44) into Equation (39) yields the total potential energy of the smeared formulation for brittle fracture:

$$\Psi_{\text{pot}} = \int_\Omega \left(h(\bar{d})\psi_0^d(\boldsymbol{\epsilon}) + \psi_0^i(\boldsymbol{\epsilon}) + \mathcal{G}_c \gamma_\ell(\bar{d}, \nabla\bar{d}) \right) \mathrm{d}V \tag{45}$$

Minimisation of Ψ_{pot} and introduction of a history field κ to enforce irreversibility [31] lead to the equilibrium equation:

$$\operatorname{div}\boldsymbol{\sigma} = \mathbf{0} \tag{46}$$

and

$$h'(\bar{d})\kappa + \frac{\mathcal{G}_c}{2\ell}\left(\bar{d} - 4\ell^2\nabla^2\bar{d}\right) = 0 \tag{47}$$

subject to the boundary conditions $\mathbf{n}\cdot\boldsymbol{\sigma} = \bar{\mathbf{t}}$, $\mathbf{u} = \bar{\mathbf{u}}$, $\mathbf{n}\cdot\nabla\bar{d} = 0$, with $\bar{\mathbf{t}}$ and $\bar{\mathbf{u}}$ the prescribed boundary tractions and displacements, respectively. We note that in the phase-field literature often the symbol $\mathcal{H}$ is used instead of κ to denote the history variable. The present notation is preferred, however, as it emphasises the similarity with gradient-enhanced damage models. The Cauchy stress $\boldsymbol{\sigma}$ and the driving force $\mathcal{F}$ are derived according to standard thermodynamic arguments:

$$\boldsymbol{\sigma} = \frac{\partial\psi^e}{\partial\boldsymbol{\epsilon}} = h(\bar{d})\frac{\partial\psi_0^d}{\partial\boldsymbol{\epsilon}} + \frac{\partial\psi_0^i}{\partial\boldsymbol{\epsilon}} \tag{48}$$

and

$$\mathcal{F} = -\frac{\partial\psi^e}{\partial d} = -h'(\bar{d})\kappa \tag{49}$$

with ψ^e as defined in Equation (44). The history field reads:

$$\kappa = \max\psi_0^d(\boldsymbol{\epsilon}) \tag{50}$$

3.2. Discrete format of phase-field models for brittle fracture

The spatial discretisation of the domain involves the following approximations:

$$\mathbf{u} = \mathbf{N}\mathbf{a} \quad , \quad \bar{d} = \bar{\mathbf{N}}\mathbf{d} \tag{51}$$

with $\mathbf{N}$ and $\bar{\mathbf{N}}$ containing the interpolation functions for the displacements and the phase field, respectively. The arrays $\mathbf{a}$ and $\mathbf{d}$ contain the discrete variables of the displacement

and the phase field. In order to capture possible snapback behaviour, the finite element formulation can be augmented by an arc-length solver [39]. The resulting set of coupled, nonlinear equations is linearised and solved using a Newton-Raphson iterative scheme. For the iterative change of the state vector at iteration k this gives:

$$\begin{bmatrix} \delta\mathbf{d} \\ \delta\mathbf{u} \\ \delta\lambda \end{bmatrix}_k = \begin{bmatrix} \mathbf{K}_{dd} & \mathbf{K}_{du} & \mathbf{0} \\ \mathbf{K}_{ud} & \mathbf{K}_{uu} & -\hat{\mathbf{f}}^{\text{ext}} \\ \mathbf{0}^{\mathrm{T}} & \mathbf{h}^{\mathrm{T}} & w \end{bmatrix}_{k-1}^{-1} \begin{bmatrix} -\mathbf{f}_d^{\text{int}} \\ \lambda\hat{\mathbf{f}}^{\text{ext}} - \mathbf{f}_u^{\text{int}} \\ -\varphi \end{bmatrix}_{k-1} \tag{52}$$

with

$$\mathbf{f}_d^{\text{int}} = \int_\Omega \left[\mathcal{G}_c \left(\frac{1}{2\ell}\mathbf{N}^{\mathrm{T}}\mathbf{N}^{\mathrm{T}} + 2\ell\mathbf{B}^{\mathrm{T}}\mathbf{B}^{\mathrm{T}} \right)\mathbf{d} + h'(\bar{d})\kappa\mathbf{N}^{\mathrm{T}} \right] \mathrm{d}V \tag{53}$$

$$\mathbf{f}_u^{\text{int}} = \int_\Omega \mathbf{B}^{\mathrm{T}} \left(h(\bar{d})\mathbf{D}^d + \mathbf{D}^i \right) \mathbf{B}^{\mathrm{T}}\mathbf{u}\mathrm{d}V \tag{54}$$

$$\varphi = \frac{1}{2}\hat{\mathbf{f}}^{\text{ext}}\left(\lambda_0\Delta\mathbf{u} - \Delta\lambda\mathbf{u}_0\right) - \Delta\tau \tag{55}$$

$$\mathbf{K}_{dd} = \frac{\partial\mathbf{f}_d^{\text{int}}}{\partial\mathbf{d}} \;,\; \mathbf{K}_{du} = \frac{\partial\mathbf{f}_d^{\text{int}}}{\partial\mathbf{u}} \;,\; \mathbf{K}_{ud} = \frac{\partial\mathbf{f}_u^{\text{int}}}{\partial\mathbf{d}} \;,\; \mathbf{K}_{uu} = \frac{\partial\mathbf{f}_u^{\text{int}}}{\partial\mathbf{u}} \;,\; \mathbf{h} = \frac{\partial\varphi}{\partial\mathbf{u}} \;,\; w = \frac{\partial\varphi}{\partial\lambda} \tag{56}$$

where $\hat{\mathbf{f}}^{\text{ext}}$ is the normalised load vector, λ is the load factor, $\Delta\tau$ is the arc length, and $\mathbf{D}^d$ and $\mathbf{D}^i$ correspond to the damaged and intact parts of the elasticity matrix, respectively. λ_0 and $\mathbf{u}_0$ are the converged values for the load factor and displacements of the previous increment.

3.3. Internal length scale and degradation function

To assess the impact of the internal length scale parameter ℓ and the degradation function g we consider the one-dimensional bar of Figure 10. The bar has a reduced thickness in the centre and is loaded at the right edge by a force $\lambda\hat{f}$. The Young's modulus is $E = 10$MPa and the fracture toughness $\mathcal{G}_c = 0.1$N/mm. The bar has a length $L = 1$mm and a thickness $b = 1$mm. The default value of the internal length scale parameter is taken as $\ell = \frac{L}{20}$. Since the problem is one-dimensional, $\psi_0^d = E$ and $\psi_0^i = 0$. Hence, the degradation function h directly acts on the Young's modulus E.

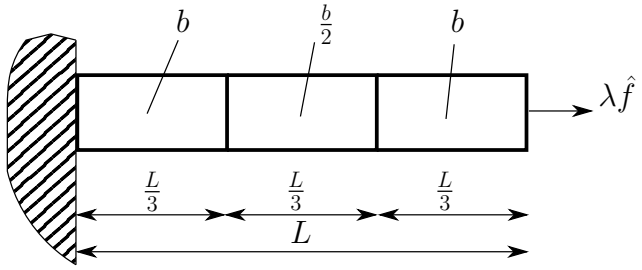

Figure 10: 1D tension test for a bar with a reduced thickness in the centre

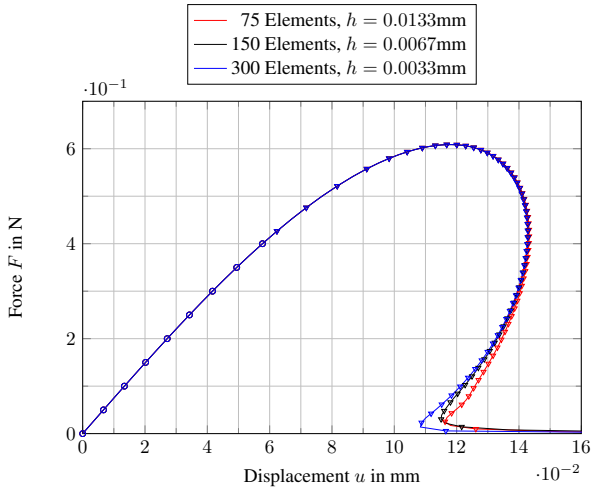

Figure 11: Mesh refinement study for a constant length scale ℓ = 0.05mm. The circles denote loading steps where force control has been used and the triangles denote the steps where arc-length control has been used

The dependence on the length scale ℓ is shown in Figure 12 for a constant mesh size (150 elements, h_{elem} = 0.0067mm), which respects the rule of thumb $\ell > h_{\text{elem}}$ to accurately approximate the crack topology [30]. Clearly, an increasing length scale results in a decreasing peak force. This makes it difficult to interpret the length scale parameter for the brittle model. While ℓ has been introduced on purely mathematical ground, independent from the mechanical field problem, these simulations show that the length scale parameter should be interpreted as a material parameter, cf [38].

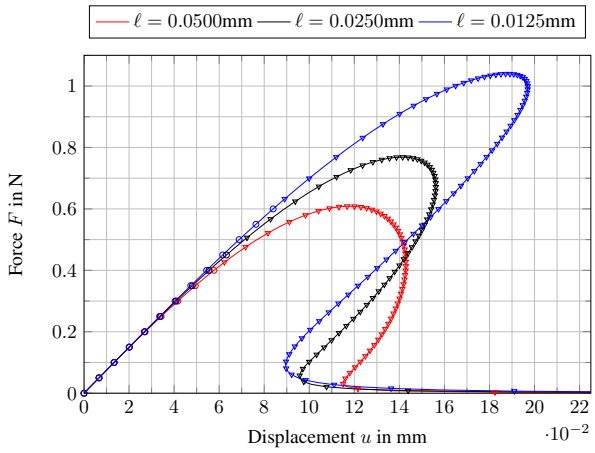

Figure 12: Influence of the length scale parameter ℓ for a constant mesh size (150 elements, h_{elem} = 0.0067mm)

Figures 11 and 12 show that the model does not exhibit linear elastic behaviour

prior to brittle fracture. Instead, the curves show nonlinearity from the onset of loading. Therefore, a cubic degradation function has been proposed [40],

$$h(\bar{d}) = s((1-\bar{d})^3 - (1-\bar{d})^2) + 3(1-\bar{d})^2 - 2(1-\bar{d})^3 \tag{57}$$

which can result in an almost linear behaviour prior to failure. The drawback is that an additional parameter s is introduced. The quadratic and the cubic degradation functions are compared in Figure 13 using different values for s.

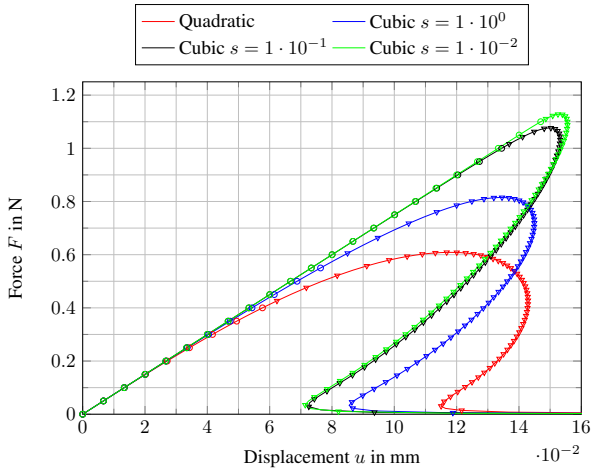

Figure 13: Comparison of the quadratic and cubic degradation functions

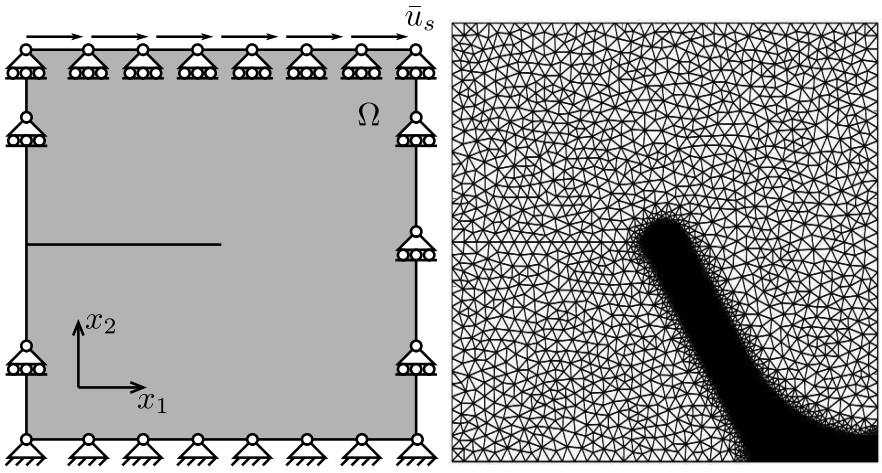

Figure 14: Problem setup and finite element mesh for the single edge notched pure shear test.

3.4. Two-dimensional example

We consider the single-edge notched specimen of Figure 14 with pure shear boundary conditions. A prescribed horizontal displacement, $\bar{u}_s$, is applied to the top boundary. Plane-strain conditions and linear elasticity have been assumed with the Lamé parameters $\lambda = 121.15\,\mathrm{kN/mm^2}$ and $\mu = 80.77\,\mathrm{kN/mm^2}$. The critical energy release rate $\mathcal{G}_c = 2.7 \cdot 10^{-3}\,\mathrm{kN/mm}$. The fracture length scale is equal to $\ell = 0.015\,\mathrm{mm}$. To accurately capture the evolution of the phase field, the mesh is refined along the anticipated crack path, Figure 14. In phase-field models for brittle fracture the length scale must be taken as small as possible to obtain an accurate approximation to the underlying linear elastic fracture mechanics problem. Evidently, very fine grids are then required. In this case, the characteristic element size in this refinement region $h_{\mathrm{elem}} = \ell/4 = 0.00375\,\mathrm{mm}$, which results in 26,472 elements.

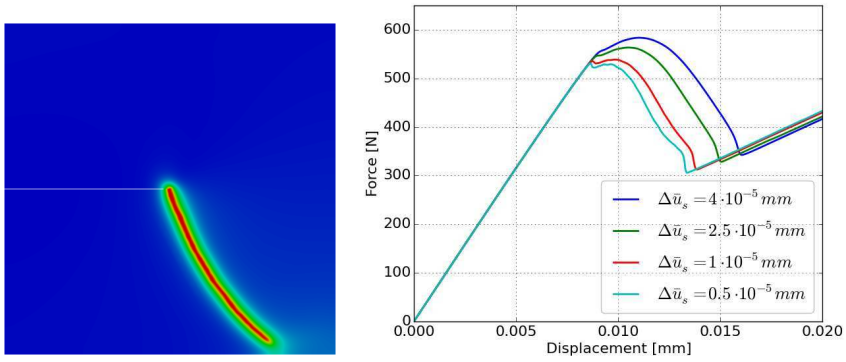

Figure 15: Phase-field solution and staggered solution algorithm step size study for the single edge notched pure shear test

Figure 15 gives the solution when the shear crack has developed almost completely. The force-displacement diagrams are shown for various step sizes. The overestimation of the amount of dissipated energy for large step sizes is a direct consequence of the employed staggered solution procedure [41]. Most noteworthy, however, is that, different from the gradient-damage model, the crack does not broaden in the wake of the crack tip upon propagation.

4. Gradient-damage models and phase-field models for fracture: similarities and differences

4.1. The diffusion equation in gradient-damage models

The Euler-Lagrange equations that govern the phase-field evolution are, cf. Equation (47):

$$\bar{d} - 4\ell^2\nabla^2\bar{d} = -\frac{2\ell h'(\bar{d})\kappa}{\mathcal{G}_c} \tag{58}$$

where implicit use has been made of the natural boundary condition $\boldsymbol{n}_\Gamma \cdot \nabla \bar{d} = 0$. In the context of phase-field models for fracture this can be interpreted as a condition requiring cracks to be perpendicular to the external boundaries of the domain. The history parameter κ obeys the Kuhn-Tucker loading-unloading conditions with the loading function defined as

$$f(\boldsymbol{\epsilon}, \kappa) = \psi_0^d(\boldsymbol{\epsilon}) - \kappa \tag{59}$$

The partial differential equation that governs the evolution of the phase field, Equation (58), is closely related to gradient-damage models. In fact, when defining the local damage field as

$$d = -\frac{2\ell h'(\bar{d})\kappa}{\mathcal{G}_c} \tag{60}$$

and the gradient parameter g as

$$g = (2\ell)^2 \tag{61}$$

the implicit form of the damage equation (19) is recovered:

$$\bar{d} - g\nabla^2 \bar{d} = d$$

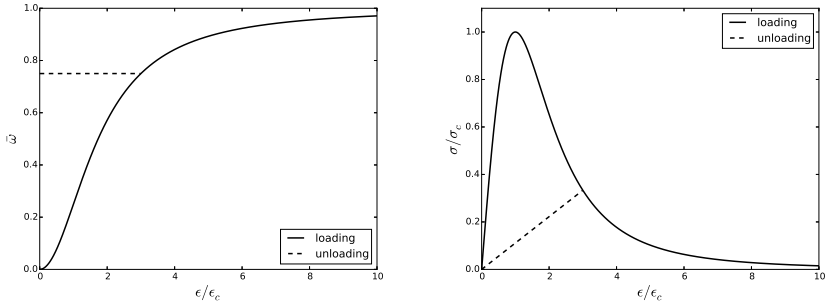

Figure 16: Homogeneous solution to the one-dimensional phase-field formulation in brittle fracture for the degradation function $h(\bar{d}) = (1 - \bar{d})^2$

4.2. One-dimensional solution for phase-field models under homogeneous deformations

The behavior of the phase-field model can further be illustrated from the homogeneous solution to the one-dimensional problem. Taking $\psi_0^d = \frac{1}{2}E\epsilon^2$, $\sigma = E\epsilon$ and $h(\bar{d}) = (1 - \bar{d})^2$, the homogeneous solution to Equation (58) shown in Figure 16 is obtained. Hence, after a sufficient amount of damage has accumulated, i.e. for $\bar{d}_c = \frac{1}{4}$, a critical load level is reached, with

$$\sigma_c = \frac{9}{16}\sqrt{\frac{\mathcal{G}_c E}{6\ell}} \qquad\qquad \epsilon_c = \sqrt{\frac{\mathcal{G}_c}{6\ell E}} \tag{62}$$

after which softening occurs. In the phase-field formulation unloading occurs using a secant stiffness, similar to damage models. From the expression for the critical stress

it is clear that when the internal length scale ℓ goes to zero, the critical stress goes to infinity. This behavior of the phase-field model correctly replicates linear elastic fracture mechanics, which is also not capable of nucleating fractures in the absence of singularities.

4.3. The driving force

As discussed, a marked difference between gradient-enhanced damage models and the phase-field approach to brittle fracture is the observation that the latter class of models does not lead to a broadening of the damage zone in the wake of the tip of the fracture process zone. This can be directly explained when comparing the expressions that result from the driving force, defined in Equation (49).

For damage models the degradation function typically has the format

$$h(\bar{d}) = 1 - \bar{d} \tag{63}$$

Substitution into Equation (49) then results in:

$$\mathcal{F} = \kappa \tag{64}$$

Hence, $\mathcal{F}$ does not vanish at complete loss of integrity, i.e. when $\bar{d} = 1$, which explains the continued broadening of the damage zone. This is different for phase-field models. Indeed, the conditions that are imposed on the degradation function, in particular Equation $(41)_3$, make that the driving force vanishes when $\bar{d} = 1$. For instance, the quadratic degradation function of Equation (42),

$$h(\bar{d}) = (1 - \bar{d})^2 \tag{65}$$

results in:

$$\mathcal{F} = (1 - \bar{d})\kappa \tag{66}$$

which becomes zero when $\bar{d} = 1$, and ensures a constant band width in the wake of the crack tip.

5. Concluding remarks

The damage-based gradient-damage and the phase-field formulations are almost identical in terms of their mathematical structure, and therefore the difference between gradient-damage models and phase-field models is mainly in their interpretation. Whereas in gradient-damage models the left-hand side of Equation (19) can be interpreted as a spatial averaging operator, the left-hand side in phase-field models, Equation (58), follows from the regularised energy variation due to fracture evolution. The right-hand-side in Equation (19) can therefore be interpreted as a local damage field, while that in Equation (58) mimicks the thermodynamic driving force for the smeared fracture. It is in this right-hand side that the most relevant differences enter between gradient-damage models and phase-field models for brittle fracture. From Equation (60) we observe that the phase-field formulation naturally introduces a length scale into the driving force for the damage field. In combination with the vanishing

derivative of the degradation function at complete loss of integrity this ensures that, once a phase field fracture has fully developed, it does not broaden. Equation (60) suggests that the vanishing derivative of the degradation function is key to driving the internal length scale to zero, which closely resembles a strategy proposed in gradient-damage modeling to avoid damage zone broadening [35].

References

[1] D. Ngo, A.C. Scordelis, Finite element analysis of reinforced concrete beams, Journal of the American Concrete Institute 64 (1967) 152–163.

[2] A. R. Ingraffea, V. Saouma, Numerical modelling of discrete crack propagation in reinforced and plain concrete. In: Fracture Mechanics of Concrete, Martinus Nijhoff Publishers, Dordrecht, 1985, pp. 171–225.

[3] G.T. Camacho, M. Ortiz, Computational modeling of impact damage in brittle materials, International Journal of Solids and Structures 33 (1996) 1267-1282.

[4] T. Belytschko, T. Black, Elastic crack growth in finite elements with minimal remeshing, International Journal for Numerical Methods in Engineering 45 (1999) 601–620.

[5] N. Moës, N. Dolbow, T. Belytschko, A finite element method for crack growth without remeshing International Journal for Numerical Methods in Engineering 46 (1999) 131–150.

[6] G.N. Wells and L.J. Sluys, A new method for modeling cohesive cracks using finite elements, International Journal for Numerical Methods in Engineering 50 (2001) 2667–2682.

[7] J.J.C. Remmers, R. de Borst, A. Needleman, A cohesive segments method for the simulation of crack growth, Computational Mechanics 31 (2003) 69–77.

[8] J. Réthoré, R. de Borst, M.-A. Abellan, A two-scale approach for fluid flow in fractured porous media, International Journal for Numerical Methods in Engineering 75 (2007) 780–800.

[9] C.V. Verhoosel, M.A. Scott, T.J.R. Hughes, R. de Borst, An isogeometric analysis approach to gradient damage models, International Journal for Numerical Methods in Engineering 86 (2011) 115–134.

[10] M. Ortiz, Y. Leroy, A. Needleman, A finite element method for localized failure analysis, Computer Methods in Applied Mechanics and Engineering 61 (1987) 189–214.

[11] T. Belytschko, J. Fish, B.E. Engelman, A finite element method with embedded localization zones, Computer Methods in Applied Mechanics and Engineering 70 (1988) 59–89.

[12] J.C. Simo, J. Oliver, F. Armero, An analysis of strong discontinuities induced by strain softening in rate-independent inelastic solids, Computational Mechanics 12 (1993) 277–296.

[13] M. Jirasek, Comparative study on finite elements with embedded discontinuities, Computer Methods in Applied Mechanics and Engineering 188 (2000) 307–330.

[14] A. Needleman, Material rate dependence and mesh sensitivity in localization problems, Computer Methods in Applied Mechanics and Engineering 67 (1987) 68–85.

[15] L.J. Sluys, R. de Borst, Wave propagation and localisation in a rate-dependent cracked medium—model formulation and one-dimensional examples, International Journal of Solids and Structures 29 (1992) 2945–2958.

[16] E. Cosserat and F. Cosserat Théorie des Corps Deformables. Herman et fils, Paris, 1909.

[17] R. de Borst, Simulation of strain localisation: a reappraisal of the Cosserat continuum, Engineering Computations 8 (1991) 317–332.

[18] R. de Borst, A generalisation of J_2-flow theory for polar continua, Computer Methods in Applied Mechanics and Engineering 103 (1993) 347–362.

[19] G. Pijaudier-Cabot, Z.P. Bažant, Nonlocal damage theory, ASCE Journal of Engineering Mechanics 113 (1987) 1512–1533.

[20] E.C. Aifantis, On the microstructural origin of certain inelastic models, Transactions ASME Journal of Engineering Materials Technologies 106 (1984) 326–330.

[21] R. de Borst, H.B. Mühlhaus, Gradient-dependent plasticity: formulation and algorithmic aspects, International Journal for Numerical Methods in Engineering 35 (1992) 521–539.

[22] R.H.J. Peerlings, R. de Borst, W.A.M. Brekelmans, H.P.J. de Vree, Gradient-enhanced damage for quasi-brittle materials. International Journal for Numerical Methods in Engineering 39 (1996) 3391–3403.

[23] R. de Borst, A. Benallal A, O.M. Heeres, A gradient-enhanced damage approach to fracture, Journal de Physique IV C6 (1996) 491–502.

[24] C. Comi, Computational modelling of gradient-enhanced damage in quasi-brittle materials, Mechanics of Cohesive-frictional Materials 4 (1999) 17–36.

[25] R.H.J. Peerlings, M.G.D. Geers, R. de Borst, W.A.M. Brekelmans, A critical comparison of nonlocal and gradient-enhanced softening continua, International Journal of Solids and Structures 38 (2001) 7723–7746.

[26] G.A. Francfort, J.-J. Marigo, Revisiting brittle fracture as an energy minimization problem, Journal of the Mechanics and Physics of Solids 46 (1998) 1319–1342.

[27] B. Bourdin, G.A. Francfort, J.-J. Marigo, Numerical experiments in revisited brittle fracture, Journal of the Mechanics and Physics of Solids 48 (2000) 797–826.

[28] B. Bourdin, G.A. Francfort, J.-J. Marigo, The variational approach to fracture, Journal of Elasticity 91 (2008) 5–148.

[29] D. Mumford, J. Shah, Optimal approximations by piecewise smooth functions and associated variational problems, Communications in Pure and Applied Mathematics 42 (1989) 577–685.

[30] C. Miehe, F. Welschinger, M. Hofacker, Thermodynamically consistent phase-field models of fracture: Variational principles and multi-field FE implementations, International Journal for Numerical Methods in Engineering 83 (2010) 1273–1311.

[31] C. Miehe, M. Hofacker, F. Welschinger, A phase field model for rate-independent crack propagation: Robust algorithmic implementation based on operator splits, Computer Methods in Applied Mechanics and Engineering 199 (2010) 2765–2778.

[32] M.J. Borden, C.V. Verhoosel, M.A. Scott, T.J.R. Hughes, C.M. Landis, A phase-field description of dynamic brittle fracture, Computer Methods in Applied Mechanics and Engineering 217–220 (2012) 77–95.

[33] M. Hofacker, C. Miehe, A phase field model of dynamic fracture: Robust field updates for the analysis of complex crack patterns, International Journal for Numerical Methods in Engineering 93 (2013) 276–301.

[34] C.V. Verhoosel, R. de Borst, A phase-field model for cohesive fracture, International Journal for Numerical Methods in Engineering 96 (2013) 43–62.

[35] M.G.D. Geers, R. de Borst, W.A.M. Brekelmans, R.H.J. Peerlings, Strain-based transient-gradient damage model for failure analyses, Computer Methods in Applied Mechanics and Engineering 160 (1998) 133–153.

[36] H. Askes, J. Pamin, R. de Borst, Dispersion analysis and element-free Galerkin solutions of second and fourth-order gradient-enhanced damage models, International Journal for Numerical Methods in Engineering 49 (2000) 811–832.

[37] A.V. Vuong, C. Giannelli, B. Jüttle, B. Simeon, A hierarchical approach to adaptive local refinement in isogeometric analysis, Computer Methods in Applied Mechanics and Engineering 200 (2011) 3554–3567.

[38] H. Amor, J.-J. Marigo, C. Maurini, Regularized formulation of the variational brittle fracture with unilateral contact: Numerical experiments, Journal of the Mechanics and Physics of Solids 57 (2009) 1209–1229.

[39] R. de Borst, M.A. Crisfield, J.J.C. Remmers, C.V. Verhoosel, Nonlinear Finite Element Analysis of Solids and Structures. John Wiley & Sons, Chichester, 2012.

[40] M.J. Borden, Isogeometric Analysis of Phase-Field Models for Dynamic Brittle and Ductile Fracture. PhD Thesis, The University of Texas at Austin (2012).

[41] J. Vignollet, S. May, R. de Borst, C.V. Verhoosel, Phase-field models for brittle and cohesive fracture, Meccanica 49 (2014) 2587–2601.